

# Electron beam-induced nanopores in Bernal-stacked hexagonal boron nitride

Cite as: Appl. Phys. Lett. **117**, 023102 (2020); <https://doi.org/10.1063/5.0010891>

Submitted: 15 April 2020 . Accepted: 26 June 2020 . Published Online: 13 July 2020

Mehmet Dogan , S. Matt Gilbert, Thang Pham, Brian Shevitski, Peter Ercius , Shaul Aloni, Alex Zettl, and Marvin L. Cohen



View Online



Export Citation



CrossMark

Lock-in Amplifiers  
up to 600 MHz



# Electron beam-induced nanopores in Bernal-stacked hexagonal boron nitride

Cite as: Appl. Phys. Lett. **117**, 023102 (2020); doi: [10.1063/5.0010891](https://doi.org/10.1063/5.0010891)

Submitted: 15 April 2020 · Accepted: 26 June 2020 ·

Published Online: 13 July 2020



View Online



Export Citation



CrossMark

Mehmet Dogan,<sup>1,2</sup>  S. Matt Gilbert,<sup>1,2,3</sup> Thang Pham,<sup>1,2,3,4</sup> Brian Shevitski,<sup>1,2,3,5</sup> Peter Ercius,<sup>5</sup>  Shaul Aloni,<sup>5</sup> Alex Zettl,<sup>1,2,3,a)</sup> and Marvin L. Cohen<sup>1,2,a)</sup>

## AFFILIATIONS

<sup>1</sup>Department of Physics, University of California, Berkeley, California 94720, USA

<sup>2</sup>Materials Sciences Division, Lawrence Berkeley National Laboratory, Berkeley, California 94720, USA

<sup>3</sup>Kavli Energy NanoScience Institute at the University of California, Berkeley, and the Lawrence Berkeley National Laboratory, Berkeley, California 94720, USA

<sup>4</sup>Department of Materials Science and Engineering, University of California, Berkeley, California 94720, USA

<sup>5</sup>Molecular Foundry, Lawrence Berkeley National Laboratory, Berkeley, California 94720, USA

<sup>a)</sup>Authors to whom correspondence should be addressed: [azettl@berkeley.edu](mailto:azettl@berkeley.edu) and [mlcohen@berkeley.edu](mailto:mlcohen@berkeley.edu)

## ABSTRACT

Controlling the size and shape of nanopores in two-dimensional materials is a key challenge in applications such as DNA sequencing, sieving, and quantum emission in artificial atoms. We here experimentally and theoretically investigate triangular vacancies in (unconventional) Bernal-stacked AB-*h*-BN formed using a high-energy electron beam. Due to the geometric configuration of AB-*h*-BN, triangular pores in different layers are aligned, and their sizes are controlled by the duration of the electron irradiation. Interlayer covalent bonding at the vacancy edge is not favored, as opposed to what occurs in the more common AA'-stacked BN. A variety of monolayer, concentric, and bilayer pores in the bilayer AB-*h*-BN are observed in high-resolution transmission electron microscopy and characterized using *ab initio* simulations. Bilayer pores in AB-*h*-BN are commonly formed and grow without breaking the bilayer character. Nanopores in AB-*h*-BN exhibit a wide range of electronic properties, ranging from half-metallic to non-magnetic and magnetic semiconductors. Therefore, because of the controllability of the pore size, the electronic structure is also highly controllable in these systems and can potentially be tuned for particular applications.

Published under license by AIP Publishing. <https://doi.org/10.1063/5.0010891>

Vacancy defects in two-dimensional materials are zero-dimensional features that can impart optical and electronic properties (e.g., bandgaps, charge state, and electron scattering behavior) to the host material, which are very different from those of the pristine sheets, and they can change the emergent measurable properties of the material (e.g., resistivity and tensile strength).<sup>1–5</sup> Moreover, such vacancies represent a physical structure in which there may be a small hole (i.e., nanopore) in an otherwise impermeable membrane.

Advances in atomic-resolution imaging and large-scale synthesis of two-dimensional materials have resulted in a rapid increase in the understanding of vacancy defects in these materials.<sup>6–8</sup> These vacancies have been studied in both naturally occurring and artificially produced forms.<sup>2,9–14</sup> The fundamental properties of vacancy defects in two-dimensional materials have led to their investigation in numerous research directions, including DNA sequencing,<sup>15–20</sup> quantum emission,<sup>21</sup> and molecular sieving.<sup>22–27</sup>

Vacancy size and geometry are critical for determining the utility of nanopores. While high-energy electron beams and ion beams have

been used to create the smallest pores observed, the shape and size of the nanopores are limited by the beam geometry.<sup>14,18,28,29</sup> In graphene, for example, the pore size has traditionally been limited to 3 nm or greater, and its shapes can only be minimally controlled.<sup>18</sup> This has been overcome in *h*-BN by leveraging the intrinsic etching properties of the material. When *h*-BN is exposed to an 80 kV electron irradiation in TEM, vacancies are etched, and atomically precise edges are formed along the nitrogen zig-zag direction,<sup>6,10,30–37</sup> which is generally thought to be caused by the difference in the electron knock-on energy thresholds of boron atoms (74 kV) and nitrogen atoms (84 kV).<sup>10,11,30,38,39</sup>

The computed atomic structure of a boron monovacancy in the monolayer *h*-BN is shown in Fig. 1(a). After its formation, under continuing electron irradiation, one of the under-coordinated nitrogen atoms adjacent to the vacancy gets ejected, followed by its neighboring boron atoms, which results in a triangular tetravacancy with a nitrogen edge. Maintaining the electron irradiation further results in progressively larger triangular vacancies.<sup>35,37,39,40</sup> This mechanism provides a robust method of creating nanopores that are equilateral triangles with

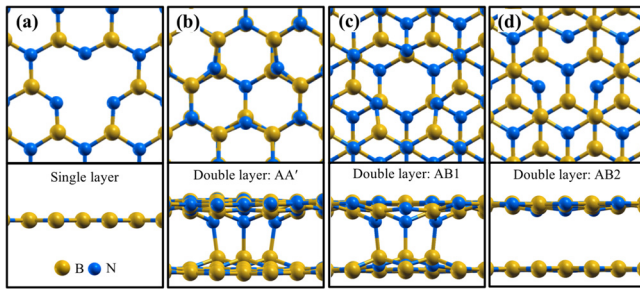


**FIG. 1.** Relaxed atomic structure of a boron monovacancy in (a) monolayer, (b) bilayer AA', (c) bilayer AB1, and (d) bilayer AB2-h-BN. For each structure, the top and side views of the atomic configuration are presented. The calculations are conducted in electron-rich conditions (three extra electrons per  $5 \times 5$  cell).

the desired size by controlling the duration of the irradiation. The size, in turn, determines the electronic structure of these triangular pores, resulting in metallic, half-metallic, or semiconducting edge regions.<sup>41–47</sup>

However, the ability to control the nanopore shape and size does not extend to samples thicker than a monolayer in the conventional AA'-stacked *h*-BN (AA'-*h*-BN). As we will demonstrate, Bernal-stacked *h*-BN (AB-*h*-BN) does not have this impediment, enabling us to create triangular pores, both in a single layer of a thicker sample and in multiple layers with concentric or fully aligned pore edges. We will describe how this is achieved and characterize the electronic properties of these pores using first-principles calculations.

In multilayer *h*-BN, the vacancy defects can interact with the adjacent layers,<sup>3,4</sup> which can affect the types and shapes of vacancies in the sheets. In AA'-*h*-BN, interlayer interactions can dominate the properties of its electron-beam-induced defects. Out-of-plane covalent bonds form across layers at the boron monovacancy sites in bilayers.<sup>3</sup> Also, along the edges of larger vacancies, covalent bonds form between the layers and the edge relaxes to resemble an *h*-BN nanotube with a small radius of curvature.<sup>4</sup>

Each lattice site in AA'-*h*-BN contains a boron directly under a nitrogen; thus, interlayer covalent bonds are available at each site in the crystal. When a B monovacancy is formed, some or all of the three under-coordinated N atoms neighboring the vacancy may form bonds with the B atoms directly underneath [Fig. 1(b)]. We find that in the electron-rich regime (three extra electrons per  $5 \times 5$  cell as in Ref. 3), forming these interlayer bonds is energetically favorable, with two out of three bonds being the most favorable configuration (Table S1). Therefore, the shape of the vacancy is not fully determined by its size, and the three-fold rotational symmetry of the lattice may be lost, which has been observed in AA'-*h*-BN.<sup>3</sup> When all three of the interlayer bonds are formed, the vacancy becomes a semiconductor, losing the half-metallic character of the B monovacancy edge (Fig. S1). Furthermore, in the AA'-*h*-BN, the second layer is obtained from the first layer by a  $60^\circ$  rotation; thus, the triangular pores with an N edge in successive layers are not aligned, and multilayer pores do not have a pre-determined shape (Fig. S2). This is consistent with the observations in Refs. 6, 10, and 30.

In Ref. 40, we described a synthesis technique for reliably producing AB-*h*-BN. For this stacking sequence, only half of the atoms are part of boron-nitrogen stacks. In Figs. 1(c) and 1(d), we present the structure of a boron monovacancy in one layer of the double layer AB-*h*-BN. As opposed to the AA' stacking, in AB-*h*-BN, the two layers

are inequivalent: in Fig. 1(c), the B atoms in the top layer are aligned with the hollow sites in the bottom layer, whereas the B atoms in the bottom layer are aligned with the N atoms in the top layer. Thus, a vacancy in the top layer yields a different configuration from a vacancy in the bottom layer. In order to consider vacancies only in the top layer, we can flip the system over if the vacancy is in the bottom layer and give the resulting stacking a different name [AB1 for Fig. 1(c) and AB2 for Fig. 1(d)]. The two stacking sequences are physically equivalent, and any vacancy configuration in one can be obtained in the other by rotating the system by  $180^\circ$  around an armchair direction. Distinguishing AB1 and AB2 allows us to meaningfully distinguish a top layer and a bottom layer in the discussions that follow.

In AB1-*h*-BN, a B monovacancy in the top layer creates three under-coordinated N atoms that are directly on top of the B atoms from the bottom layer, which yields an interlayer bonding in the electron-rich regime, as in the AA' case [Fig. 1(c) and Table S1]. However, in AB2-*h*-BN, the under-coordinated N atoms lack a neighbor directly underneath, and thus the top layer stays flat and no new bonds form [see Fig. 1(d)]. Decoupling the two layers retains the magnetic properties of each layer, the half-metallic nature of the B monovacancy in the top layer (Fig. S1).

In general, when the two layers remain chemically decoupled, their single-layer electronic and magnetic properties are retained, which can allow for the size-dependent magnetism found in the single-layer *h*-BN nanopores to exist within a multilayer structure without disturbance. In Fig. 2, we summarize the dependence of the magnetic properties on the pore size based on our calculations. For the B monovacancy (pore size: 1) [Fig. 2(a)], each of the three neighboring N atoms is magnetized. For the pore that consists of 3 B and 1 N vacancy (tetravacancy, pore size: 2) [Fig. 2(b)], magnetism is zero due to the dimerization of the corner N atoms. For larger pores (pore size: 3, 4, 5, ...), all the non-corner edge N atoms are magnetized and the corners remain dimerized [Figs. 2(c) and 2(d)]. Each magnetized N atom carries a magnetization of approximately  $1 \mu_B$  (the exact values for the edge N are printed in Fig. 2, and see Tables S2 and S3 for the remaining values carried by the neighboring atoms in certain cases). Therefore, the total magnetization (in  $\mu_B$ ) of a pore is  $M_{\text{total}} \cong 3, 0, 3, 6, 9, 12, \dots$  for pore sizes 1, 2, 3, and so on.

To experimentally realize these pores in multilayer *h*-BN, we grow AB-*h*-BN using chemical vapor deposition (CVD) on Cu and Fe substrates and fabricate nanopores using an 80 kV electron beam (see the supplementary material for further details). Studying our AB-*h*-BN samples using a high-resolution transmission electron microscopy (HRTEM) focal series reconstruction,<sup>3,6,40</sup> we find many monolayer vacancies in two-layer stacks. Figure 3 shows three such monolayer vacancies in the phase of the reconstructed exit wave. Assuming that the pores are formed in the top layer, the first one corresponds to the AB2 stacking with a boron monovacancy [Fig. 3(a)]. In the second one, a tetravacancy is formed in the top layer of an AB1 bilayer [Fig. 3(b)]. The third one corresponds to a larger nanopore with 10 B and 6 N atoms missing from the top layer in the bilayer AB2-*h*-BN [Fig. 3(c)]. The relaxed theoretical structures (which contain no interlayer covalent bonds) match the experimental HRTEM structure almost exactly, as shown in the middle row (simulated HRTEM exit waves based on the DFT-computed coordinates are presented in Fig. S3). Spin-resolved DFT calculations result in different characterizations for these vacancies: half-metal with a total

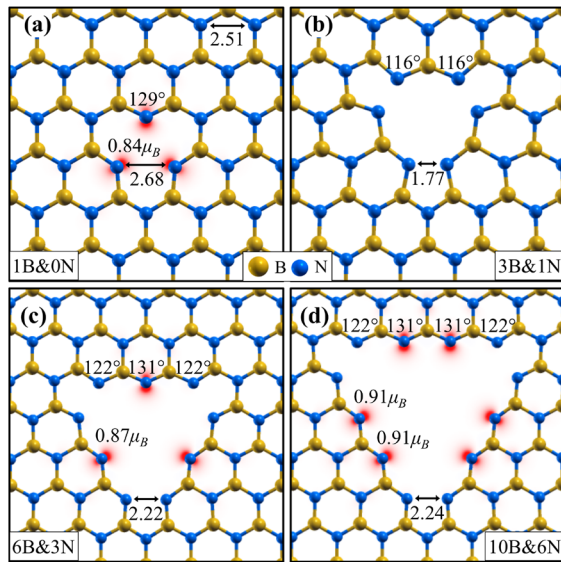


**FIG. 2.** N-terminated triangular nanopores in the single-layer *h*-BN with (a) pore size: 1, (b) pore size: 2, (c) pore size: 3, and (d) pore size: 4. For each case, the spatial distribution of the computed magnetization is also plotted. For significantly magnetized atoms, the magnetization values (computed by decomposing the Löwdin charges on the atomic orbitals) are printed next to the representative atoms (there is a threefold symmetry in each case). Some important angles and distances (in Å) are also shown.

magnetization of  $3.26 \mu_B$  [Fig. 3(a)]; non-magnetic semiconductor with two sharp in-gap states 1.8 eV and 2.2 eV above the valence band maximum [Fig. 3(b)]; and magnetic semiconductor with gaps of 0.6 eV and 0.2 eV for the two spin channels and a total magnetization of  $6.00 \mu_B$  [Fig. 3(c)].

This result suggests that tuning the vacancy size in AB-*h*-BN is a reliable method for tuning its magnetic and electronic properties. The ability to create vacancies with tunable bandgaps in the visible range may be useful for *h*-BN in optoelectronics and photon emission applications.<sup>21,48</sup>

In a multilayer AB-*h*-BN sample, because there is no relative rotation between layers,<sup>40</sup> the triangular pores with an N edge are parallel regardless of which layer they are in, which is not the case for AA'-*h*-BN (Fig. S2). After a monolayer triangular vacancy is formed, if the electron irradiation is maintained, a triangular vacancy tends to form in the exposed region of the other layer, resulting in nested triangular vacancies. Figure S4 shows the growth of a vacancy in a monolayer of *h*-BN as it merges with a larger vacancy in the next layer to form a bilayer nanopore: When a small one- or few-atom vacancy forms within a triangular monolayer region that is embedded within a bilayer area, first, two of its edges align with the large vacancy to form bilayer edges, then the third edge aligns to form a “bilayer pore,” and then the bilayer pore grows while retaining its bilayer edges and triangular geometry.

A possible mechanism that leads to this inclination to form bilayer edges is that a covalent bond forms between the edge atoms. In this scenario, as the triangular vacancies in the top and bottom *h*-BN layers intersect, the edge atoms covalently bond together. This would form a stable edge that maintains its structure as it is irradiated and reforms as it is etched. Below, we take a closer look at the bilayer edges to examine this hypothesis, as well as alternate mechanisms.

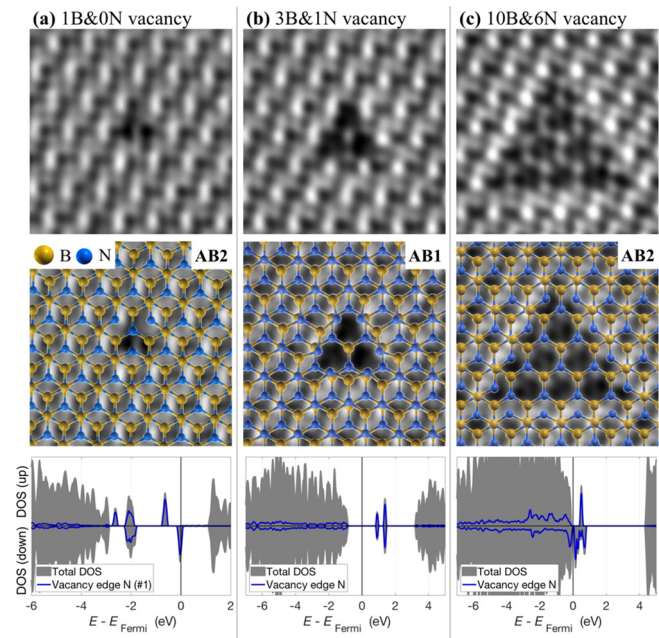


**FIG. 3.** Top row: the phase of HRTEM focal series reconstructions of vacancies produced in a single layer of a bilayer AB-stacked *h*-BN, composed of (a) 1 B atom, (b) 3 B and 1 N atoms, and (c) 10 B and 6 N atoms. Each field-of-view is 2 nm wide. Middle row: the same images with the computed atomic structures overlaid. Bottom row: computed spin-resolved density of state (DOS) plots. The total DOS is plotted as gray areas, and the blue curves are obtained by adding up the DOS projected onto the 2s and 2p orbitals of the under-coordinated N atoms at the vacancy edges.

We have performed HRTEM on bilayer triangular pores and edges in the bilayer AB-*h*-BN and found that when we are able to identify atoms and stacks of atoms in a bilayer edge image, we systematically obtain the same edge configuration. In Fig. 4, we present a representative image for this configuration. Figure 4(a) shows an overview of two 3 nm bilayer vacancies in the AB stacked *h*-BN as highlighted by the green triangles. Multiple smaller monolayer vacancies are also present. The edge highlighted by the blue dashed box is presented in Fig. 4(b). In order to investigate any potential lattice relaxation in the structures, we overlay a grid that has spacings  $a_0/2$  in the *x*-direction and  $\sqrt{3}a_0/4$  in the *y*-direction, where  $a_0$  is the lattice constant. All of the atomic positions for the undisturbed lattice fall on this grid, as shown in Fig. 4(c). We observe that the double-atom stacks of boron and nitrogen (brightest peaks in the image) exactly fall on the grid of the undisturbed lattice, independent of how close they are to the edge [Fig. 4(b)]. This indicates that the interlayer relaxation and covalent bond formation are unlikely in these bilayer edges. We note that we are not always able to identify atoms and stacks of atoms in the HRTEM images of bilayer edges, and thus we do not entirely rule out other configurations.

To further understand these bilayer edges, we have computed possible edge structures. The best candidate for the bilayer edge in Fig. 4 is presented in Fig. S5. In this “open edge” case, two monolayer edges sit on top of one another without interlayer bonding. Other types of bilayer edges may also be present in these systems, and our calculations regarding them, including some “closed edge”

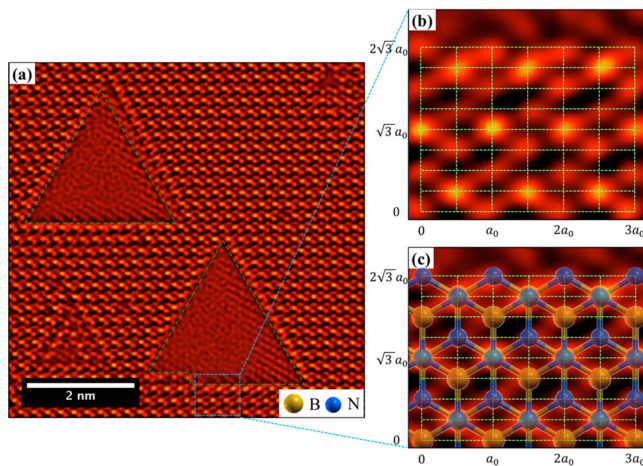


**FIG. 4.** (a) HRTEM focal series reconstruction image of triangular vacancies produced in *h*-BN under an 80 kV electron irradiation. Two  $\sim 3$ -nm bilayer pores (highlighted in green) are present with several smaller monolayer vacancies. The image is presented using a high-contrast filter to distinguish between vacuum (black and dim red), single boron atoms (bright red dots), and stacks of boron and nitrogen (brighter yellowish dots). (b) A zoomed-in section of the edge highlighted by the blue dashed box in (a). An overlaid grid denotes the atomic positions for the undisturbed bilayer *h*-BN lattice. (c) The same zoomed-in section of the edge from (a) with the atomic species in an undisturbed lattice overlaid.

cases, will be presented in a future report. The unrelaxed grid of positions is overlaid on the open edge structure as in Fig. 4, showing that in-plane distortions are negligible. In previous computational studies, the nitrogen-terminated zigzag edge of the BN monolayer was found to be half-metallic.<sup>43,49</sup> Looking at the projected density of state (PDOS) plots in Fig. S5, we observe that the open bilayer edge preserves the half-metallic character of the monolayer edge, with a magnetization of  $2.02 \mu_B$  per cell along the edge direction, localized on the edge N atoms (localization of the magnetization is depicted in Fig. S5).

Since closed edges are not regularly observed in our images, they are not the explanation of why the pores preferentially form a bilayer edge. We suggest that the explanation may be that bare monolayers of *h*-BN are less stable under electron irradiation. A second layer may provide protection from chemical sputtering from the electron beam or may increase the kinetic scattering threshold for the layers. Thus, whenever a small monolayer region of *h*-BN is exposed, the layer is etched back to form a bilayer edge. Therefore, the formation of bilayer edges in *AB*-*h*-BN appears to be due to the kinetic effects, whereas, in *AA'*-*h*-BN, bilayer edges occur because of the stabilizing interlayer bonds. As a result, the bilayer edges in *AB*-*h*-BN greatly differ from the bilayer edges in the *AA'*-stacked BN, which are insulating and have large in-plane and out-of-plane relaxations.<sup>4</sup> This is an important difference as it suggests that *AB*-*h*-BN could potentially be used for its 1D conducting edges.

We have achieved the controlled formation of triangular vacancies in multilayer *h*-BN, using a growth technique that results in Bernal stacking (*AB*-*h*-BN). Due to the favorability of nitrogen terminated vacancy edges in BN and the lack of relative rotation between the layers in Bernal stacking, triangular pores in different layers are aligned in *AB*-*h*-BN. We have shown that the interlayer covalent bonding following vacancy formation in a layer is not favored for this

stacking sequence, increasing the level of controllability and symmetry in these pores. Furthermore, we observe that pores with bilayer edges are preferentially formed, which is most likely not due to the interlayer covalent bonds but rather the kinetic effects. We observe a variety of monolayer and bilayer pores in the bilayer *AB*-*h*-BN in our HRTEM focal series reconstructions and find excellent matches from theoretical simulations. These pores have a variety of electronic properties, ranging from half-metallic to semiconducting, which is encouraging for future research toward many applications such as DNA sequencing, molecular sieving, and quantum emitters.

See the [supplementary material](#) for details of the experimental and theoretical methods, three supplementary tables, and five supplementary figures.

## AUTHORS' CONTRIBUTIONS

M.D. and S.M.G. contributed equally to this work.

This work was supported primarily by the Director, Office of Science, Office of Basic Energy Sciences, Materials Sciences and Engineering Division, of the U.S. Department of Energy under Contract No. DE-AC02-05-CH11231, within the *sp*<sup>2</sup>-bonded Materials Program (No. KC2207), which supported TEM imaging and first-principles computations of the atomic structures. Sample growth was supported by the Director, Office of Science, Office of Basic Energy Sciences, Materials Sciences and Engineering Division, of the U.S. Department of Energy under Contract No. DE-AC02-05-CH11231, within the van der Waals Heterostructures Program (No. KCWF16). Further support for the theoretical work was provided by the NSF Grant No. DMR-1926004, which supported first-principles computations of the precise electronic structures. Computational resources were provided by the DOE at the Lawrence Berkeley National Laboratory's NERSC facility and the NSF through XSEDE resources at NICS. S.M.G. acknowledges support from the Kavli Energy NanoSciences Institute Fellowship and the NSF Graduate Fellowship Program. M.D. thanks Sehoon Oh and P.E. thanks Earl J. Kirkland for their helpful scientific discussions.

## DATA AVAILABILITY

The data that support the findings of this study are available from the corresponding author upon reasonable request.

## REFERENCES

- V. Iberi, L. Liang, A. V. Ievlev, M. G. Stanford, M.-W. Lin, X. Li, M. Mahjour-Samani, S. Jesse, B. G. Sumpter, S. V. Kalinin, D. C. Joy, K. Xiao, A. Belianinov, and O. S. Ovchinnikova, "Nanoforging single layer MoSe<sub>2</sub> through defect engineering with focused helium ion beams," *Sci. Rep.* **6**(1), 30481 (2016).
- J.-H. Chen, G. Autès, N. Alem, F. Gargiulo, A. Gautam, M. Linck, C. Kisielowski, O. V. Yazyev, S. G. Louie, and A. Zettl, "Controlled growth of a line defect in graphene and implications for gate-tunable valley filtering," *Phys. Rev. B* **89**(12), 121407 (2014).
- N. Alem, O. V. Yazyev, C. Kisielowski, P. Denes, U. Dahmen, P. Hartel, M. Haider, M. Bischoff, B. Jiang, S. G. Louie, and A. Zettl, "Probing the out-of-plane distortion of single point defects in atomically thin hexagonal boron nitride at the picometer scale," *Phys. Rev. Lett.* **106**(12), 126102 (2011).
- N. Alem, Q. M. Ramasse, C. R. Seabourne, O. V. Yazyev, K. Erickson, M. C. Sarahan, C. Kisielowski, A. J. Scott, S. G. Louie, and A. Zettl, "Subangstrom

- edge relaxations probed by electron microscopy in hexagonal boron nitride," *Phys. Rev. Lett.* **109**(20), 205502 (2012).
- <sup>5</sup>D. Halbertal, M. B. Shalom, A. Uri, K. Bagani, A. Y. Meltzer, I. Marcus, Y. Myasoedov, J. Birkbeck, L. S. Levitov, A. K. Geim, and E. Zeldov, "Imaging resonant dissipation from individual atomic defects in graphene," *Science* **358**(6368), 1303–1306 (2017).
- <sup>6</sup>N. Alem, R. Erni, C. Kisielowski, M. D. Rossell, W. Gannett, and A. Zettl, "Atomically thin hexagonal boron nitride probed by ultrahigh-resolution transmission electron microscopy," *Phys. Rev. B* **80**(15), 155425 (2009).
- <sup>7</sup>H. I. Rasool, C. Ophus, and A. Zettl, "Atomic defects in two dimensional materials," *Adv. Mater.* **27**(38), 5771–5777 (2015).
- <sup>8</sup>Ç. Ö. Girit, J. C. Meyer, R. Erni, M. D. Rossell, C. Kisielowski, L. Yang, C.-H. Park, M. F. Crommie, M. L. Cohen, S. G. Louie, and A. Zettl, "Graphene at the edge: Stability and dynamics," *Science* **323**(5922), 1705–1708 (2009).
- <sup>9</sup>A. V. Krashenninikov and F. Banhart, "Engineering of nanostructured carbon materials with electron or ion beams," *Nat. Mater.* **6**(10), 723–733 (2007).
- <sup>10</sup>J. C. Meyer, A. Chuvilin, G. Algara-Siller, J. Biskupek, and U. Kaiser, "Selective sputtering and atomic resolution imaging of atomically thin boron nitride membranes," *Nano Lett.* **9**(7), 2683–2689 (2009).
- <sup>11</sup>N. Alem, R. Erni, C. Kisielowski, M. D. Rossell, P. Hartel, B. Jiang, W. Gannett, and A. Zettl, "Vacancy growth and migration dynamics in atomically thin hexagonal boron nitride under electron beam irradiation," *Phys. Status Solidi RRL* **5**(8), 295–297 (2011).
- <sup>12</sup>A. L. Gibb, N. Alem, J.-H. Chen, K. J. Erickson, J. Ciston, A. Gautam, M. Linck, and A. Zettl, "Atomic resolution imaging of grain boundary defects in monolayer chemical vapor deposition-grown hexagonal boron nitride," *J. Am. Chem. Soc.* **135**(18), 6758–6761 (2013).
- <sup>13</sup>T. P. Pham, A. P. Goldstein, J. O. Lewicki, S. Kucheyev, C. P. Wang, T. A. Russell, M. Worsley, L. Woo, W. Mickelson, and A. Zettl, "Nanoscale structure and superhydrophobicity of sp<sup>2</sup>-bonded boron nitride aerogels," *Nanoscale* **7**(23), 10449–10458 (2015).
- <sup>14</sup>A. W. Robertson, G.-D. Lee, K. He, C. Gong, Q. Chen, E. Yoon, A. I. Kirkland, and J. H. Warner, "Atomic structure of graphene subnanometer pores," *ACS Nano* **9**(12), 11599–11607 (2015).
- <sup>15</sup>S. J. Heerema and C. Dekker, "Graphene nanodevices for DNA sequencing," *Nat. Nanotechnol.* **11**(2), 127–136 (2016).
- <sup>16</sup>D. Deamer, M. Akesson, and D. Branton, "Three decades of nanopore sequencing," *Nat. Biotechnol.* **34**(5), 518–524 (2016).
- <sup>17</sup>T. Haynes, I. P. S. Smith, E. J. Wallace, J. L. Trick, M. S. P. Sansom, and S. Khalid, "Electric-field-driven translocation of ssDNA through hydrophobic nanopores," *ACS Nano* **12**(8), 8208–8213 (2018).
- <sup>18</sup>S. Garaj, S. Liu, J. A. Golovchenko, and D. Branton, "Molecule-hugging graphene nanopores," *Proc. Natl. Acad. U. S. A.* **110**(30), 12192–12196 (2013).
- <sup>19</sup>C. A. Merchant, K. Healy, M. Wanunu, V. Ray, N. Peterman, J. Bartel, M. D. Fischbein, K. Venta, Z. Luo, A. T. C. Johnson, and M. Drndić, "DNA translocation through graphene nanopores," *Nano Lett.* **10**(8), 2915–2921 (2010).
- <sup>20</sup>G. F. Schneider, S. W. Kowalczyk, V. E. Calado, G. Pandraud, H. W. Zandbergen, L. M. K. Vandersypen, and C. Dekker, "DNA translocation through graphene nanopores," *Nano Lett.* **10**(8), 3163–3167 (2010).
- <sup>21</sup>T. T. Tran, K. Bray, M. J. Ford, M. Toth, and I. Aharonovich, "Quantum emission from hexagonal boron nitride monolayers," *Nat. Nanotechnol.* **11**(1), 37–41 (2016).
- <sup>22</sup>S. P. Koenig, L. Wang, J. Pellegrino, and J. S. Bunch, "Selective molecular sieving through porous graphene," *Nat. Nanotechnol.* **7**(11), 728–732 (2012).
- <sup>23</sup>J. Zhao, G. He, S. Huang, L. F. Villalobos, M. Dakhchoune, H. Bassas, and K. V. Agrawal, "Etching gas-sieving nanopores in single-layer graphene with an angstrom precision for high-performance gas mixture separation," *Sci. Adv.* **5**(1), eaav1851 (2019).
- <sup>24</sup>S. C. O'Hern, M. S. H. Boutilier, J.-C. Idrobo, Y. Song, J. Kong, T. Laoui, M. Atieh, and R. Karnik, "Selective ionic transport through tunable subnanometer pores in single-layer graphene membranes," *Nano Lett.* **14**(3), 1234–1241 (2014).
- <sup>25</sup>M. Heiranian, A. B. Farimani, and N. R. Aluru, "Water desalination with a single-layer MoS<sub>2</sub> nanopore," *Nat. Commun.* **6**(1), 8616 (2015).
- <sup>26</sup>L. Wang, L. W. Drahushuk, L. Cantley, S. P. Koenig, X. Liu, J. Pellegrino, M. S. Strano, and J. S. Bunch, "Molecular valves for controlling gas phase transport made from discrete angstrom-sized pores in graphene," *Nat. Nanotechnol.* **10**(9), 785–790 (2015).
- <sup>27</sup>P. R. Kidambi, D. Jang, J.-C. Idrobo, M. S. H. Boutilier, L. Wang, J. Kong, and R. Karnik, "Nanoporous atomically thin graphene membranes for desalting and dialysis applications," *Adv. Mater.* **29**(33), 1700277 (2017).
- <sup>28</sup>C. J. Russo and J. A. Golovchenko, "Atom-by-atom nucleation and growth of graphene nanopores," *Proc. Natl. Acad. U. S. A.* **109**(16), 5953–5957 (2012).
- <sup>29</sup>D. Emmrich, A. Beyer, A. Nadzeyka, S. Bauerdick, J. C. Meyer, J. Kotakoski, and A. Götzhäuser, "Nanopore fabrication and characterization by helium ion microscopy," *Appl. Phys. Lett.* **108**(16), 163103 (2016).
- <sup>30</sup>J. Kotakoski, C. H. Jin, O. Lehtinen, K. Suenaga, and A. V. Krashenninikov, "Electron knock-on damage in hexagonal boron nitride monolayers," *Phys. Rev. B* **82**(11), 113404 (2010).
- <sup>31</sup>C. Jin, F. Lin, K. Suenaga, and S. Iijima, "Fabrication of a freestanding boron nitride single layer and its defect assignments," *Phys. Rev. Lett.* **102**(19), 195505 (2009).
- <sup>32</sup>J. H. Warner, M. H. Rummeli, A. Bachmatiuk, and B. Büchner, "Atomic resolution imaging and topography of boron nitride sheets produced by chemical exfoliation," *ACS Nano* **4**(3), 1299–1304 (2010).
- <sup>33</sup>J. S. Kim, K. B. Borisenko, V. Nicolosi, and A. I. Kirkland, "Controlled radiation damage and edge structures in boron nitride membranes," *ACS Nano* **5**(5), 3977–3986 (2011).
- <sup>34</sup>G. H. Ryu, H. J. Park, J. Ryou, J. Park, J. Lee, G. Kim, H. S. Shin, C. W. Bielawski, R. S. Ruoff, S. Hong, and Z. Lee, "Atomic-scale dynamics of triangular hole growth in monolayer hexagonal boron nitride under electron irradiation," *Nanoscale* **7**(24), 10600–10605 (2015).
- <sup>35</sup>S. M. Gilbert, G. Dunn, A. Azizi, T. Pham, B. Shevitski, E. Dimitrov, S. Liu, S. Aloni, and A. Zettl, "Fabrication of subnanometer-precision nanopores in hexagonal boron nitride," *Sci. Rep.* **7**(1), 15096 (2017).
- <sup>36</sup>A. G. Rajan, K. S. Sillmore, J. Swett, A. W. Robertson, J. H. Warner, D. Blankschtein, and M. S. Strano, "Addressing the isomer cataloguing problem for nanopores in two-dimensional materials," *Nat. Mater.* **18**(2), 129–135 (2019).
- <sup>37</sup>O. Mouhoub, R. Martinez-Gordillo, J. Nelayah, G. Wang, J.-H. Park, K. K. Kim, Y. H. Lee, C. Bichara, A. Loiseau, C. Ricolleau, H. Amara, and D. Alloyeau, "Quantitative insights into the growth mechanisms of nanopores in hexagonal boron nitride," *Phys. Rev. Mater.* **4**(1), 014005 (2020).
- <sup>38</sup>A. Zobelli, A. Gloter, C. P. Ewels, G. Seifert, and C. Colliex, "Electron knock-on cross section of carbon and boron nitride nanotubes," *Phys. Rev. B* **75**(24), 245402 (2007).
- <sup>39</sup>T. Pham, A. L. Gibb, Z. Li, S. M. Gilbert, C. Song, S. G. Louie, and A. Zettl, "Formation and dynamics of electron-irradiation-induced defects in hexagonal boron nitride at elevated temperatures," *Nano Lett.* **16**(11), 7142–7147 (2016).
- <sup>40</sup>S. M. Gilbert, T. Pham, M. Dogan, S. Oh, B. Shevitski, G. Schumm, S. Liu, P. Ercius, S. Aloni, M. L. Cohen, and A. Zettl, "Alternative stacking sequences in hexagonal boron nitride," *2D Mater.* **6**(2), 021006 (2019).
- <sup>41</sup>R.-F. Liu and C. Cheng, "Ab initio studies of possible magnetism in a BN sheet by nonmagnetic impurities and vacancies," *Phys. Rev. B* **76**(1), 014405 (2007).
- <sup>42</sup>M. S. Si and D. S. Xue, "Magnetic properties of vacancies in a graphitic boron nitride sheet by first-principles pseudopotential calculations," *Phys. Rev. B* **75**(19), 193409 (2007).
- <sup>43</sup>F. Zheng, G. Zhou, Z. Liu, J. Wu, W. Duan, B.-L. Gu, and S. B. Zhang, "Half metallicity along the edge of zigzag boron nitride nanoribbons," *Phys. Rev. B* **78**(20), 205415 (2008).
- <sup>44</sup>A. Du, Y. Chen, Z. Zhu, R. Amal, G. Q. M. Lu, and S. C. Smith, "Dots versus anti-dots: Computational exploration of structure, magnetism, and half-metallicity in boron–nitride nanostructures," *J. Am. Chem. Soc.* **131**(47), 17354–17359 (2009).
- <sup>45</sup>L.-C. Yin, H.-M. Cheng, and R. Saito, "Triangle defect states of hexagonal boron nitride atomic layer: Density functional theory calculations," *Phys. Rev. B* **81**(15), 153407 (2010).
- <sup>46</sup>O. Cretu, Y.-C. Lin, M. Koshino, L. H. G. Tizei, Z. Liu, and K. Suenaga, "Structure and local chemical properties of boron-terminated tetravacancies in hexagonal boron nitride," *Phys. Rev. Lett.* **114**(7), 075502 (2015).
- <sup>47</sup>J. Ryou, J. Park, and S. Hong, "Investigations of vacancy structures related to their growth in H-BN sheet," *Nanoscale Res. Lett.* **12**(1), 445 (2017).
- <sup>48</sup>S. Choi, T. T. Tran, C. Elbadawi, C. Lobo, X. Wang, S. Juodkazis, G. Seniutinas, M. Toth, and I. Aharonovich, "Engineering and localization of quantum emitters in large hexagonal boron nitride layers," *ACS Appl. Mater. Interfaces* **8**(43), 29642–29648 (2016).
- <sup>49</sup>V. Barone and J. E. Peralta, "Magnetic boron nitride nanoribbons with tunable electronic properties," *Nano Lett.* **8**(8), 2210–2214 (2008).